BUTTERWORTH HEINEMANN

Polymer Vol. 36 No. 20, pp. 3889–3897, 1995

0032-3861/95/$10.00 + 0.00

Crystallization of poly(ethylene oxide) in binary blends containing poly(*p*-vinyl phenol)

P. Pedrosa, J. A. Pomposo, E. Calahorra and M. Cortázar*
Departamento de Ciencia y Tecnología de Polímeros, Facultad de Ciencias Químicas de San Sebastián, PO Box 1072, San Sebastián, Spain
(Received 24 June 1993; revised 19 July 1994)

Blends of poly(ethylene oxide) (PEO) with an amorphous polymer, poly(*p*-vinyl phenol) (PVPh), showed a single, composition-dependent, glass transition temperature as a consequence of the miscibility between components. X-ray diffraction and differential scanning calorimetry (d.s.c.) results indicated a strong reduction of blend crystallinity with increasing PVPh content. Observation of melting point depression allowed the determination of the interaction energy density, B, between the two polymers in the melt. To obtain equilibrium melting point data, the Hoffman–Weeks procedure was employed to take into account the influence of crystal morphology. The values of B obtained by d.s.c. and by thermal optical microscopy were -7.1 and $-8.8\,\mathrm{cal\,cm^{-3}}$, respectively. Analysis of the isothermal crystallization by means of the Avrami equation led to average values of the Avrami index of 2.5 for both pure PEO and a PEO/PVPh 90/10 blend, and 3.1 for the remaining compositions analysed. The temperature and composition dependence of the growth rates were analysed using an expression incorporating both the diffusion mechanism and the nucleation tendency. A discontinuity in the temperature coefficient of the growth rate curve was found for PEO/PVPh blends with 90 and 80 wt% PEO. The experimental results indicate that the rate of crystallization, the degree of crystallinity and the equilibrium melting temperature are strongly dependent on the composition of the blends.

(Keywords: semicrystalline blends; poly(ethylene oxide); poly(*p*-vinyl phenol))

INTRODUCTION

The widespread potential applications for polymer blends have led in recent years to an increased research effort on both miscibility[1–3] and crystallization, especially on the kinetics of the latter[4–6]. This interest is related to the widespread industrial use of these materials and to the theoretical complexity of the mixing process. It is well known that a useful way of improving the impact strength, toughness and ductility properties of an amorphous polymer is to blend it with a crystalline one. Crystalline, glassy or even rubbery phases can coexist in amorphous/crystalline blends depending on the thermal treatment, allowing a large variety of morphologies to be attained for specific technological uses.

In the case of blends in which one of the components is crystalline, the miscibility of the system involves a decrease in the equilibrium melting point of the crystalline polymer, as a function of the blend composition. The presence of this depression is often considered to be a miscibility criterion. In addition, the melting point depression of the crystalline component provides a simple method for determining the interaction energy density of the blend[7,8]. As expected, the effects of the amorphous polymer on the nucleation, crystallization kinetics and crystallinity behaviour, as well as on the morphology, are by no means negligible[9]. Recently, several aspects related to the influence of the amorphous polymer on the diffusion mechanism of secondary crystallization have been emphasized[10–12].

In this work we have selected a typical crystalline/amorphous pair: poly(ethylene oxide) (PEO) and poly(*p*-vinyl phenol) (PVPh). The first, PEO, is a highly crystalline polymer that exhibits miscibility with many chemically different polymeric materials such as poly(acrylic acid)[13], poly(methacrylic acid)[14], poly(hydroxy ether of bisphenol A)[15,16] and poly(vinyl alcohol)[17] as a consequence of strong specific interactions between the PEO and these counter-polymers. Likewise, blends of PEO with poly(methyl methacrylate) (PMMA)[18], isotactic PMMA[19], poly(vinyl acetate)[20], poly(ether sulfone)[21] and poly(*N*-vinyl pyrrolidone)[22], among others, have been the subject of several works. The study of these pairs normally concentrates on the miscibility between components, with emphasis on the PEO crystallization and the melting behaviour in the presence of the second amorphous polymer.

Poly(*p*-vinyl phenol) is a proton donor which offers excellent potential for hydrogen-bonding interactions with proton-acceptor polymers, since the hydroxyl group of the repeat unit is easily accessible in the 4-position of the aromatic ring. To our knowledge, the presence of this type of specific interaction between PVPh and PEO was first reported by Moskala *et al.*[23]. In addition, Qin *et al.*[24]

* To whom correspondence should be addressed

have studied the miscibility of this system by several techniques and concluded that the blends are miscible across the entire composition range, due to specific interactions between the hydroxyl groups of PVPh and the etheric oxygens of PEO. A further study of this system by Zhang *et al.*[25] employing high-resolution solid-state ^{13}C n.m.r. spectroscopy also indicated that intermolecular hydrogen-bonding interactions cause the blends to show macroscopic miscibility.

The aim of this work was to study the miscibility and the melting behaviour of this system, as well as the influence of PVPh on the degree of crystallinity, the kinetics of bulk crystallization and the spherulitic growth rate of PEO. The crystallization process was analysed using the Avrami equation[26–28], while the spherulitic growth data were interpreted in terms of an expression incorporating a nucleation parameter and two mobility factors that account for the diffusion step in the substrate nucleation and surface spreading process[11,12].

EXPERIMENTAL

Materials and sample preparation

Polysciences Inc. PEO ($M_w = 300\,000$) and PVPh ($M_w = 30\,000$) were used as supplied. Blends of PEO/PVPh were prepared by casting films from 2% (w/v) tetrahydrofuran (THF) solutions at 323 K. Special care was taken to remove the solvent from the films. Thus, samples were dried in a vacuum oven at 333 K for 2 weeks, heated at 423 K for 3 h (under vacuum) and subsequently slowly cooled to room temperature. This thermal treatment allowed us to recover the glass transition temperature (T_g) of the initial dried PVPh, which was found to be significantly depressed when residual THF remains in the sample. The validity of the above procedure was further supported by means of thermogravimetric measurements.

Specimens for crystallinity measurements were prepared as plates by compression moulding the samples at 393 K for 5 min. Crystallization of the plates took place in a desiccator at room temperature and atmospheric pressure for 1 week. After that, the plates were cut into small pieces of dimensions $1.8 \times 15 \times 18\,mm^3$ for X-ray diffraction measurements and specimens of 6–8 mg were weighted for thermal analysis.

Wide-angle X-ray diffraction (WAXD)

X-ray diffraction data were measured with 1.54 Å ($Cu\,K_\alpha$) radiation using a Philips PW 1729 generator with a PW 1820 vertical goniometer and a graphite monochromator. WAXD patterns at elevated temperature were obtained by using a Anton-Paar K-HR variable-temperature attachment.

The X-ray diffraction profile was analysed with a computer program that refines the crystalline diffraction peaks and the diffuse amorphous scattering of the sample, by using the amorphous halo of the completely noncrystalline specimen as a reference. The degree of crystallinity was then obtained as the ratio of the area corresponding to the crystalline peaks to the area of both the crystalline peaks and the diffuse amorphous scattering.

Differential scanning calorimetry (d.s.c.)

Glass transition, melting and overall crystallization kinetics were analysed by differential scanning calorimetry using a Perkin–Elmer DSC-2C apparatus equipped with a TADS microcomputer, and calibrated with indium. The measurements were made under a helium atmosphere since liquid nitrogen was used for cooling.

For the glass transition determination the samples were subject to the following thermal history: initially the material was heated from 150 to 423 K at 40 K min^{-1} and maintained at that temperature for 3 min to ensure a well-defined and reproducible T_g, after that it was cooled to 150 K at a nominal cooling rate of 320 K min^{-1}. The T_g (measured at the half-height of the corresponding heat capacity jump) was subsequently recorded at a heating rate of 20 K min^{-1} in a second scan.

Estimates of crystallinity were obtained from the heats of fusion of the compression-moulded specimens in a first d.s.c. scan at a heating rate of 20 K min^{-1}. The degree of crystallinity was determined by comparing the heat of fusion of the blend with that[29] for 100% crystalline PEO (2.1 kcal mol^{-1}).

The isothermal crystallization process was studied using the following procedure: the crystalline samples were melted at 373 K for 10 min to destroy all prior crystals, cooled quickly to the desired crystallization temperature, T_c, and the heat flow evolved during the overall isothermal crystallization was recorded as a function of time. To obtain the observed calorimetric melting temperatures, T_m, as a function of crystallization temperature, the samples were melted at 373 K for 10 min, quenched to the desired T_c and then maintained at T_c until the crystallization had proceeded to 10% of the overall process. In a subsequent step, the samples were heated from T_c to a temperature above the melting point at a scanning rate of 10 K min^{-1} and the melting point was determined.

Thermo-optical analysis (t.o.a.)

Melting point measurements were also conducted on a Leitz Aristomet polarizing optical microscope equipped with a Mettler FP82 hot-stage. The samples, in the form of films, were first melted at 373 K for 10 min and then quickly inserted into another hot-stage (Mettler FP52) at a pre-fixed T_c. As soon as the PEO spherulites filled the optical field, the samples were heated at a rate of 3 K min^{-1}. The melting point was taken to be the temperature at which the birefringence disappeared. Optical microscopy was also used to study the morphology and the isothermal growth rate, G, of PEO spherulites in the blends. The radius of growing spherulites was obtained by measuring the size of PEO spherulites as a function of time during isothermal crystallization. Only pure PEO, PEO/PVPh 90/10 and PEO/PVPh 80/20 blends were studied since with higher PVPh contents, the crystallization temperatures required ($T_c < 300$ K) were not accessible using the hot-stage.

Dynamic mechanical thermal analysis (d.m.t.a.)

Dynamic viscoelastic properties were measured in a Polymer Laboratories DMTA apparatus. Scans of frequency (0.3, 1, 2, 3, 5, 10, 20 and 30 Hz) at isothermal temperatures (263, 273, 283, 293, 303 and 313 K) were

Table 1 Glass transition temperatures for PEO/PVPh blends

wt% PVPh	T_g (K)	wt% PVPh	T_g (K)
0	218	50	284
10	228	60	322
20	222	70	356
30	236	80	382
35	248	90	407
40	260	100	428

Table 2 Crystallinities and heats of fusion for PEO/PVPh blends as determined by two different techniques

	Degree of crystallinity		Heat of fusion (cal/g of PEO)	
wt% PEO	WAXD	d.s.c.	WAXD[a]	d.s.c.
100	0.76	0.78	36	37
90	0.68	0.70	36	37
80	0.60	0.58	36	34
70	0.44	0.38	30	26

[a] Calculated from the WAXD crystallinity and the heat of fusion of 100% crystalline PEO[29] taking into account the blend composition

carried out in bending mode, with samples of dimensions $2 \times 15 \times 1$ mm^3. From the dynamic or complex viscosity, η^*, a master curve was constructed for each sample in order to determine the temperature dependence of the shift factor and the Williams–Landel–Ferry (WLF) apparent activation energy for viscoelastic relaxation (U^*), following standard procedures[30].

RESULTS AND DISCUSSION

Miscibility behaviour

All PEO/PVPh blends exhibited a single T_g which changed with blend composition, as summarized in *Table 1*. Consequently, it can be concluded that PEO/PVPh blends are completely miscible across the full composition range, at least at the scale probed by d.s.c. (ca. 100 Å). An analysis of the T_g–composition data in terms of the free volume theory has been reported recently[31].

WAXD and d.s.c. crystallinities

Crystallinity measurements offer a useful way to ascertain the influence of PVPh on the crystallization behaviour of PEO/PVPh blends. *Figure 1* shows the X-ray diffraction patterns for PEO/PVPh blends crystallized at atmospheric pressure and room temperature for 1 week. As the PVPh content increases, the intensity of the crystalline diffraction peaks decreases and there is a noticeable enhancement of the diffuse amorphous scattering. For the blends, the positions of the Bragg diffraction peaks do not shift significantly with respect to those of neat PEO, so no change in unit cell dimensions and hence in crystal structure is apparent. Thus, the progressive addition of PVPh results only in a continuous decrease of crystallinity as summarized in *Table 2*. Estimates of crystallinity from d.s.c. measurements are also provided in this table for comparison. As can be seen, there is a good agreement between the degree of crystallinity values determined from X-ray diffraction and d.s.c., pointing to a lack of substantial recrystallization in the d.s.c. during the heating scan. Similarly, the heats of fusion calculated from WAXD crystallinity (*Table 2*) agree well with those determined experimentally from d.s.c. For samples containing a low PVPh content, the heat of fusion per g of crystallizable polymer (*Table 2*) remains unchanged within the limits of experimental uncertainty. As the amount of

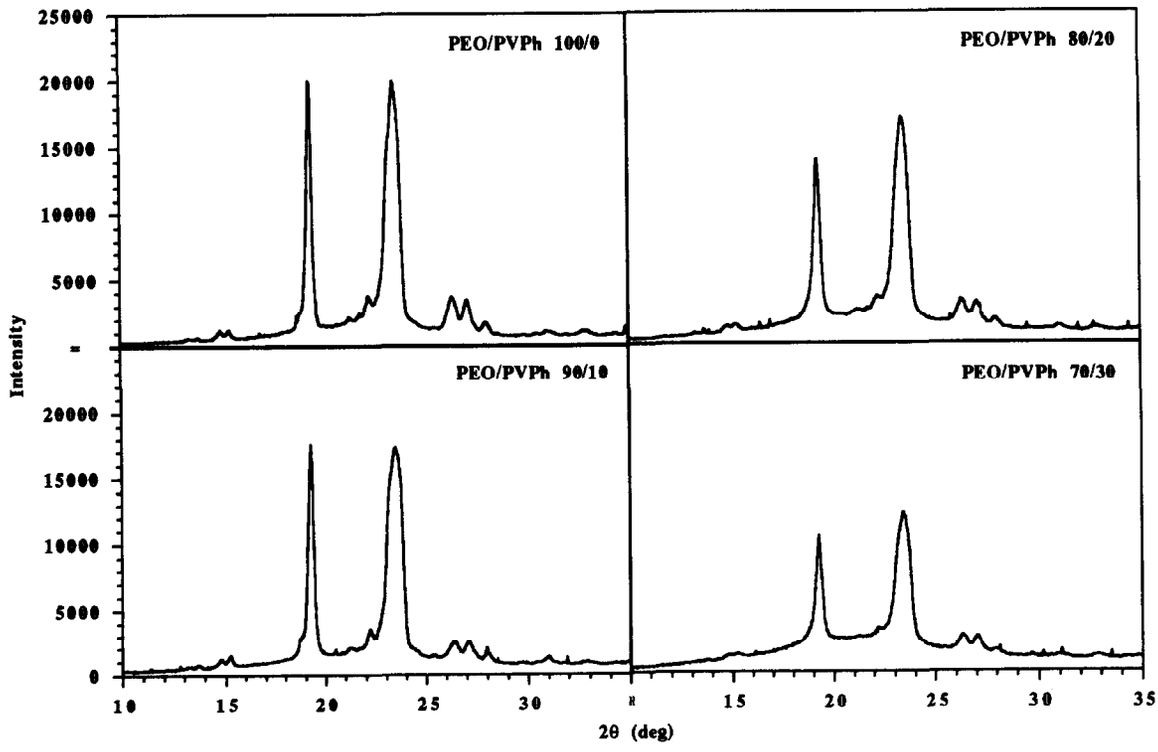

Figure 1 X-ray diffraction patterns for crystalline PEO/PVPh blends at different compositions

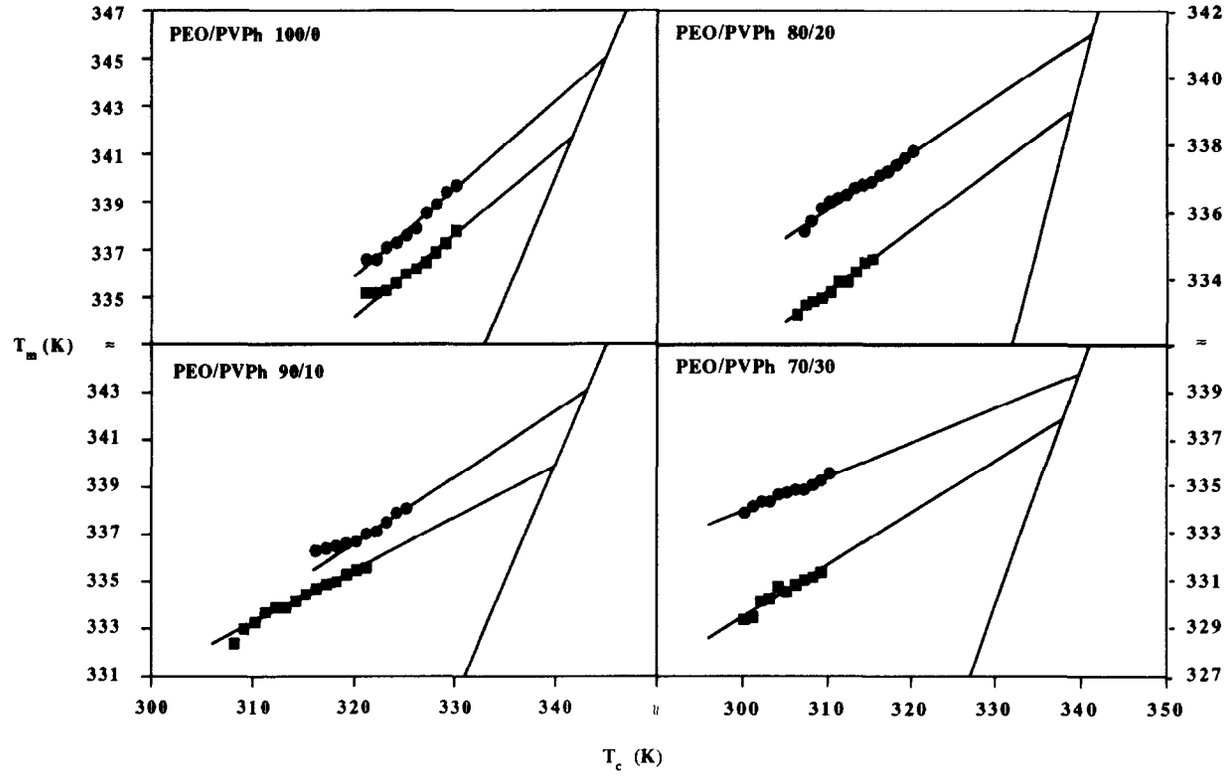

Figure 2 Hoffman–Weeks plots for PEO/PVPh blends employing data from: ■, d.s.c.; and ●, t.o.a.

PVPh is increased, the tendency to crystallize is reduced as a consequence of the increase of blend T_g (*Table 1*) that results in a lower temperature interval ($T_m - T_g$). In this sense, blends with a PVPh content higher than 40 wt% do not crystallize because, upon addition of a sufficient amount of the rigid amorphous component, the mobility of the crystallizable segments becomes insufficient to allow their diffusion to the spherulitic growth sites[24,32].

Melting behaviour and melting point depression

For miscible polymer blends where one component crystallizes, the melting point depression of the crystalline polymer can be used to evaluate the interaction energy density, B, or the related Flory χ parameter from the following equations[7].

$$(T_m^\circ)_{pure} - (T_m^\circ)_{blend} = \Delta T_m^\circ = -B\left(\frac{V_{2u}}{\Delta H_{2u}}\right)(T_m^\circ)_{pure}\,\phi_1^2 \quad (1)$$

and

$$\chi = \frac{BV_{1u}}{R(T_m^\circ)_{pure}} \quad (2)$$

where the subscripts 1 and 2 refer to the amorphous polymer and the crystalline polymer, respectively; ΔH_{2u} is the heat of fusion per mole of crystalline repeating units; V_{1u} and V_{2u} are the molar volumes of the corresponding repeat units; ϕ_1 is the volume fraction of the component 1 in the blend; and T_m° is the equilibrium melting point. Equation (1) does not take into account the combinatorial entropy of mixing, because its influence on the melting point depression can be considered negligible when one deals with blends of large molecules[33]. Accordingly, by using appropriate T_m° data, the value of B can be obtained from the slope of a plot of ΔT_m° *versus* ϕ_1^2. However, the apparent melting point depression in a blend can be due not only to thermodynamic factors, but to kinetic and morphological factors as well. The kinetic factors are related to variations in the crystal morphology as a function of blend composition. Therefore, to study the melting point depression, an adequate determination of the equilibrium melting temperatures is required in order to eliminate kinetic contributions. In the present work, equilibrium melting points have been determined according to Hoffman and Weeks' analysis[34], by means of the following equation:

$$T_m = T_m^\circ\left(1 - \frac{1}{\beta}\right) + \frac{T_c}{\beta} \quad (3)$$

where T_m is the experimental melting temperature, T_c is the crystallization temperature and $1/\beta$ is a morphological factor, which depends on the crystal thickness. Referring to equation (3), the equilibrium melting temperature is obtained by setting $T_m = T_c$, which implies the extrapolation to infinite thickness of lamella.

The melting temperatures T_m were studied by both d.s.c. and t.o.a. *Table 3* shows the equilibrium melting temperatures for pure PEO and the crystalline blends determined by means of these techniques, following the Hoffman–Weeks protocol. *Figure 2* shows the best-fit T_m *versus* T_c lines obtained for the PEO/PVPh blends*. The value of T_m° for pure PEO obtained by d.s.c. was 342 K, while the value derived from t.o.a. was 345 K.

Table 3 Melting point depression of PEO in PEO/PVPh blends as determined by two different techniques

	T_m° (K)	
wt% PEO	d.s.c.	t.o.a.
100	342	345
90	340	343
80	339	341
70	338	340
65	336	–

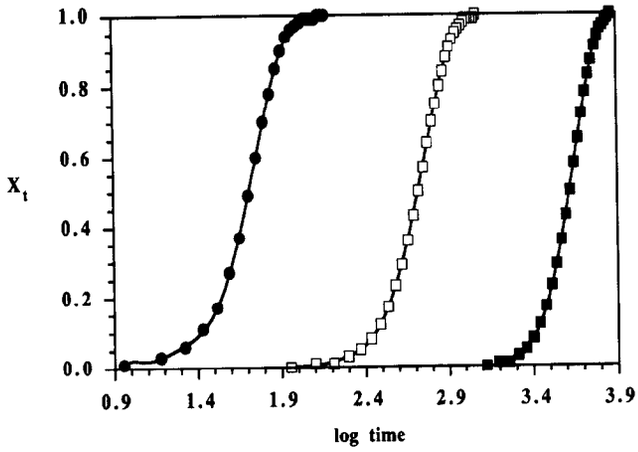

Figure 3 Crystallization isotherms for PEO/PVPh blends at $T_c = 308.8$ K: ●, 90/10; □, 80/20; ■, 70/30

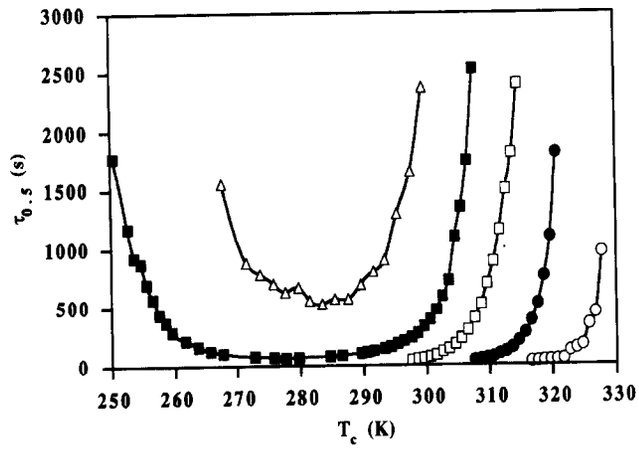

Figure 4 Half-time of crystallization *versus* crystallization temperature for PEO/PVPh blends at different compositions: ○, 100/0; ●, 90/10; □, 80/20; ■, 70/30; △, 65/35

These values are in good agreement with the values reported previously in the literature[10,36] and the slight difference between them could be attributed to the different thermal treatments employed in each experimental technique: in the d.s.c. experiments the samples were crystallized until 10% of the total crystallinity was obtained, whereas in the t.o.a. measurements they were crystallized until the optical microscopy field was filled.

When the data of *Table 3* are fitted to equation (1) (employing[29] $\Delta H_{2u} = 2.1$ kcal mol^{-1} and $V_{2u} = 38.9$ cm^3 mol^{-1}), a value of the interaction energy density of -7.1 cal cm^{-3} is obtained from d.s.c. and -8.8 cal cm^{-3} from t.o.a. These values are close to that reported previously by Qin *et al.*[24] (-10.2 cal cm^{-3}) taking into account that a low-molecular-weight PVPh and non-equilibrium melting temperatures were used by these authors. The values of B suggests that the strength of the hydrogen-bonding interactions between components is very strong and comparable to that found in the phenoxy/PEO system[16].

Overall rates of crystallization

Crystallization isotherms of PEO/PVPh blends were obtained by plotting the fraction X_t of PEO crystallized at time t against log(time). *Figure 3* shows the results for three representative PEO/PVPh blends at $T_c = 308.8$ K. As can be seen in this figure, for a given time the presence of PVPh results in a decrease of the fraction of PEO crystallized. This feature is also noticed when the half-time of crystallization $\tau_{0.5}$, defined as the time taken for half the crystallinity to develop, is plotted against T_c (see *Figure 4*). For pure PEO and the PEO/PVPh blends with 90 and 80 wt% PEO, the isothermal crystallization can be studied only in the region of high T_c because at low values the process starts before thermal equilibrium is reached in the d.s.c. Interestingly, the PEO/PVPh blends having 70 and 65 wt% PEO showed the well-known bell shape as a consequence of the two main competing factors governing the overall rate of crystallization. The first is the nucleation process, which is the controlling factor at high crystallization temperatures and causes $\tau_{0.5}$ to increase with T_c, while the second is the molecular mobility, which dominates at low crystallization temperatures so $\tau_{0.5}$ raises as T_c decreases. On the other hand, the progressive reduction of the $(T_m - T_g)$ range upon addition of PVPh is responsible for the narrow curve observed in *Figure 4* for the PEO/PVPh 65/35 blend compared with that of the PEO/PVPh 70/30 blend.

The bulk kinetics of crystallization have been analysed in terms of the Avrami equation[26–28] using the double logarithmic form:

$$\ln[-\ln(1 - X_t)] = \ln K_n + n \ln t \qquad (4)$$

where n is the Avrami index which is related to the geometry of the growth and K_n is the overall kinetic rate constant. Plots of $\ln[-\ln(1 - X_t)]$ against $\ln t$ were found to be always linear until high degrees of conversion were obtained, as shown in *Figure 5* for a PEO/PVPh 90/10 blend at several crystallization temperatures. The slope and the intercept of the straight lines allow one to determine the values of n and K_n, respectively. As can be seen in *Table 4*, the average values of the Avrami index in each blend range from 2.5 (for pure PEO and the PEO/PVPh 90/10 blend) to 3.1 (for PEO/PVPh 80/20 and PEO/PVPh 70/30 blends).

* In *Figure 2*, several data for high degrees of supercooling show departures from the best-fit T_m *versus* T_c line. For the points above this line, crystallization might have occurred prior to reaching the crystallization temperature; whereas the values below the line suggest that at the highest supercoolings the thickening process is being inhibited. In this sense, it has been recently argued by Mezghani *et al.*[35] that the disordered surface generated at very high degree of supercooling ought to present a major obstruction to the lamellar thickening process. On the other hand, a certain upward curvature in the T_m *versus* T_c data from t.o.a. is observed for the PEO/PVPh blends with 20 and 30 wt% PVPh. Such behaviour might be caused by an increased thickening rate at the lowest supercoolings. In any case, the inherent scatter of the data as well as the limited melting temperature range obtained prevent any definitive statement being made

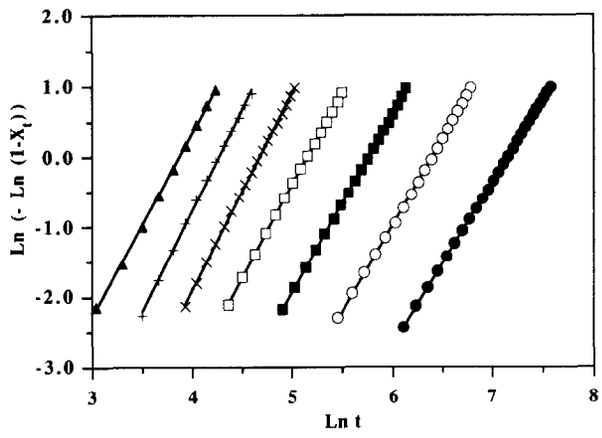

Figure 5 Avrami plots for a 90/10 PEO/PVPh blend in a selected crystallization temperature range: ▲, 307.7 K; +, 309.7 K; ×, 311.7 K; □, 313.7 K; ■, 315.7 K; ○, 317.7 K; ●, 319.7 K

Table 4 Values of the Avrami index for pure PEO and its blends with PVPh

wt% PEO	T_c (K) range	n
100	327.8–316.7	2.5
90	320.9–307.7	2.5
80	314.8–297.6	3.1
70	308.9–250.4	3.1
65	299.6–267.6	3.0

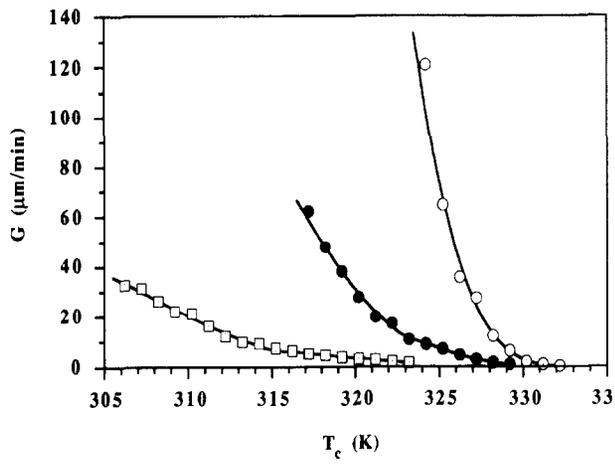

Figure 6 Dependence of the spherulite growth rate with the crystallization temperature for PEO/PVPh blends: ○, 100/0; ●, 90/10; □, 80/20

Similar values have been reported in the literature for pure PEO[16,36].

Morphology and spherulite growth rate

It is well known that PEO can be crystallized from the melt with either a spherulitic, a hedritic or an intermediate spherulite–hedrite morphology by changing the crystallization conditions appropriately. Thin films of PEO/PVPh blends isothermally crystallized in the temperature range 300.2–330.2 K showed a spherulitic morphology for all the compositions examined. Under the optical microscope, the spherulites of pure PEO and the PEO/PVPh 90/10 blends displayed a 'Maltese cross' birefringent pattern with a regular shape and defined borders. By increasing the PVPh content in the blends, the spherulites exhibited a less regular texture that could be related to the coarseness of the crystalline lamellae as a consequence of the progressive presence of uncrystallized material in the interlamellar regions[37]. Furthermore, the PEO/PVPh blend having 30 wt% PVPh showed coarse spherulites with irregular borders.

On the other hand, the spherulite radius was found to increase linearly with time for all the temperatures and blend compositions investigated. Thus, the spherulite growth rate, G, was constant until impingement took place. The dependence of G on T_c is shown in *Figure 6*. As can be seen in this figure, for a given T_c the addition of PVPh to PEO causes a depression in the G values. In the next section, the growth rate data of pure PEO and the PEO/PVPh blends are analysed in terms of secondary nucleation and molecular mobility.

Temperature dependence of G

It is well known that the spherulitic growth rate, G, of crystalline polymers is governed by the rate of secondary nucleation (i) and the rate of substrate completion (g). The physical picture usually involves the deposition of a first molecular stem on the growth front and the attachment of subsequent stems in the chain on the crystal surface[38]. Although idealized, this simple model allows one to include both the diffusion mechanism and the nucleation tendency. When the crystallization conditions are such that many deposited stems are growing simultaneously over different points on the substrate, the macroscopic growth rate can be expressed in terms of i, g and the layer thickness (b_0) as[39,40]:

$$G = b_0 (2\mathrm{gi})^{1/2} \tag{5}$$

and

$$G = b_0 (2\beta_g\beta_i)^{1/2} \exp\left(\frac{-K_g}{T_c f \Delta T}\right) \tag{6}$$

where β_i and β_g are mobility parameters that account for the diffusion step in the substrate nucleation and the surface spreading processes[11,12], respectively; K_g is the nucleation constant, T_c is the crystallization temperature; $\Delta T = T_m^\circ - T_c$ is the supercooling, and f is a correction factor given by $2T_c/(T_m^\circ + T_c)$. For a neat crystalline polymer, it has been argued that both β_i and β_g are proportional to the self-diffusion coefficient (D_s) of the polymer[11,12]. According to molecular theories of polymer melt dynamics[41,42], D_s is also proportional to the reciprocal of viscosity (η), so to a first approximation we can write

$$\beta_i \text{ and } \beta_g \propto D_s \propto \left(\frac{1}{\eta}\right) \propto \exp\left(\frac{-U^*}{R(T_c - T_\infty)}\right) \tag{7}$$

where the last term arises from the classical WLF formulation[28,43] of the temperature dependency of η, U^* being a constant characteristic of the activation energy of chain motion in the melt, R the gas constant, and T_∞ the theoretical temperature at which all motion associated with viscous flow ceases. As a consequence, for the pure crystalline polymer, equation (6) becomes

$$G = G_0 \exp\left(\frac{-U^*}{R(T_c - T_\infty)}\right) \exp\left(\frac{-K_g}{T_c f \Delta T}\right) \tag{8}$$

where G_0 is a pre-exponential factor containing quantities not strongly dependent on temperature.

For miscible blends of crystalline and amorphous polymers, the above scenario remains essentially valid, but certain modifications are needed. A simple analysis suggests that in this case the amorphous component may have a significant influence on the diffusion mechanism associated with the substrate nucleation process. Accordingly, for these systems, it is usually claimed[10–12] that β_i may be proportional to the mutual diffusion coefficient (D_m) of the blend, since two cooperative events are involved: the approach of the crystalline polymer to the crystal surface, and the rejection of the amorphous component from the growth front. By analogy to equation (7), β_i can be now formulated as follows:

$$\beta_i \propto D_m \propto \left(\frac{1}{\eta_m}\right) \propto \exp\left(\frac{-U_m^*}{R(T_c - T'_\infty)}\right) \qquad (9)$$

where η_m is the blend viscosity, U_m^* is the WLF-based activation energy related to the temperature dependence of η_m, and T'_∞ is the theoretical temperature at which the viscous flow of the blend ceases. No substantial changes can be anticipated for the surface spreading process so, for the polymer blend, β_g may still be given by equation (7). Therefore, for the blend the spherulitic growth rate may be expressed as:

$$G = G'_0 \exp\left(\frac{-U^*}{2R(T_c - T_\infty)} + \frac{-U_m^*}{2R(T_c - T'_\infty)}\right) \times \exp\left(\frac{-K'_g}{T_c f \Delta T}\right) \qquad (10)$$

where K'_g is the nucleation constant of the crystalline polymer in the blend, and the pre-exponential constant G'_0 incorporates several factors not significantly dependent on temperature. It can be shown that equation (10) reduces to equation (8) for two limiting cases: when the amount of amorphous polymer in the blend is very low, and when the addition of the amorphous component does not modify the values of K_g, T_∞ and U^*. However, it should be difficult to accept the use of a single value of U^* for a strongly interactive polymer blend system if it is truly miscible. In this sense, we have determined the WLF-type activation energies of PEO and several PEO/PVPh blends from d.m.t.a. measurements (see Experimental) and we have found that, in fact, there is a significant difference between the value of U^* corresponding to pure PEO and the values of U_m^* determined for the blends (*Table 5*). Consequently, the temperature dependence of G for neat PEO has been analysed in terms of equation (8), whereas the influence of T_c on the spherulitic growth rate of PEO/PVPh blends with 80 and 90 wt% PEO has been rationalized by means of equation (10).

The values of G_0 and K_g for PEO (*Table 6*) have been obtained from the intercept and the slope, respectively, of a conventional plot of $\ln G + U^*/[R(T_c - T_\infty)]$ *versus* $1/(T_c f \Delta T)$ which, as illustrated in *Figure 7*, can be fitted to a straight line in the T_c range investigated. We have also included for comparison in this figure several literature growth rate data[44–47] for PEO samples with M_w ranging from 1.1×10^5 to 9.9×10^5. As can be seen,

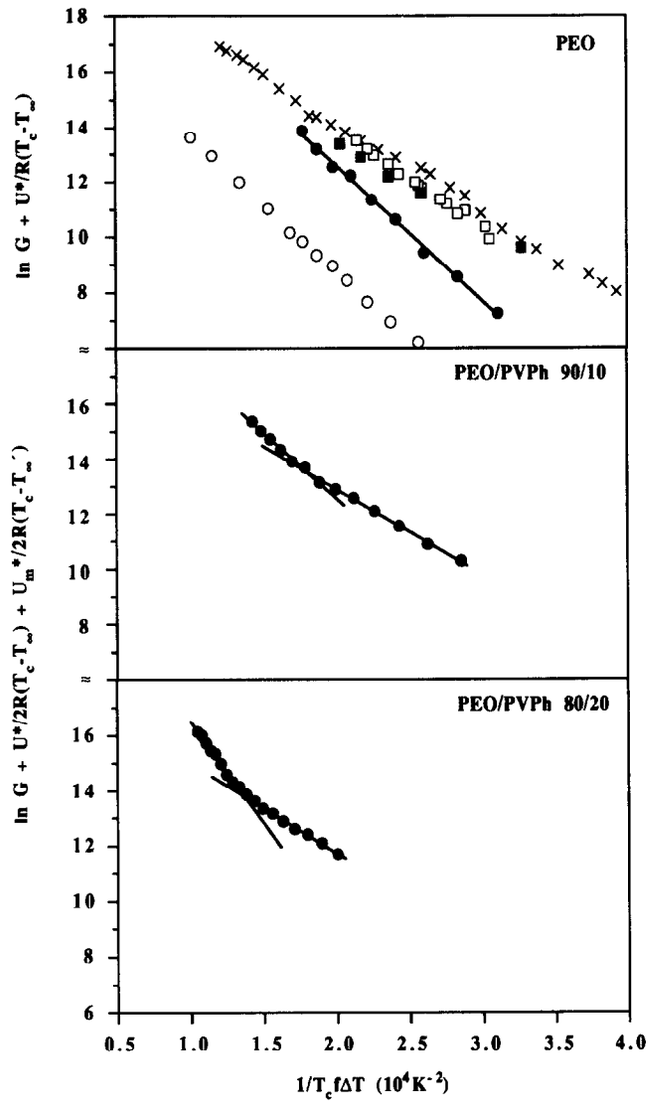

Figure 7 Kinetic analysis of the crystallization rate data for neat PEO (see text): ●, data from this work, M_w(PEO) = 3×10^5; ×, data from Cheng *et al.*[44], M_w(PEO) = 1.1×10^5; □, data from Hay and Sabir[45], M_w(PEO) = 2×10^5; ■, data from Maclaine and Booth[46], M_w(PEO) = 2.4×10^5, and ○, data from Alfonso and Russell[47], M_w(PEO) = 9.9×10^5; and for PEO/PVPh blends: ●, data from this work. T_m° values from d.s.c. has been taken from *Table 3*, U^* and U_m^* values from *Table 5* and T_g values from *Table 1*

Table 5 WLF activation energies for PEO/PVPh blends as determined by d.m.t.a. measurements

wt% PEO[a]	U_m^* (kcal mol^{-1})[b]
90	3.59
80	4.01
65	4.97

[a] For pure PEO, $U^* = 2.82$ kcal mol^{-1} was determined using $T_\infty = T_g - 50$ K
[b] Calculated using $T'_\infty = T_g - 50$ K in all cases

Table 6 Comparison of the growth rate constants for pure PEO[a] and PEO/PVPh blends

wt% PEO	T_c (K) range	$\ln(G_0/G'_0)$	K_g/K'_g
90	329.2–323.2	1.170	1.568
90	323.2–317.2	1.012	1.024
80	323.2–315.2	1.225	1.483
80	315.2–306.2	0.939	0.664

[a] Data for pure PEO: $G_0 = 9.192 \times 10^3$ cm s^{-1}; $K_g = 4.895 \times 10^4$ K^2

the slope and, hence, the nucleation constant obtained in this work is similar to that for the PEO of $M_w = 9.9 \times 10^5$, although slightly higher than those for the remaining PEO samples.

Following a similar procedure, equation (10) can be rearranged to:

$$\ln G + \frac{U^*}{2R(T_c - T_\infty)} + \frac{U_m^*}{2R(T_c - T'_\infty)} = \ln G'_0 - \frac{K'_g}{T_c f \Delta T} \quad (11)$$

in order to determine G'_0 from the intercept and K'_g from the slope of a $\ln G + U^*/[2R(T_c - T_\infty)] + U_m^*/[2R(T_c - T'_\infty)]$ *versus* $1/(T_c f \Delta T)$ plot. However, as shown in *Figure 7*, two straight lines are needed for each PEO/PVPh blend in order to reproduce accurately the experimental points. Interestingly, the same feature is also observed when $\ln G$ [instead of the l.h.s. of equation (11)] is plotted against $1/(T_c f \Delta T)$, so the break is not a consequence of the WLF-type terms employed in equation (11) to take the diffusion mechanism into account. Such a break is not observed for the neat PEO investigated in this work, for which accurate growth data cannot be obtained at crystallization temperatures below 324.2 K due to experimental limitations as a consequence of the small crystallization times involved (see *Figure 4*). For the blends, the slope change in the secondary nucleation plot can be reasonably attributed to a change in the crystallization regime or in the crystallographic direction of the growth front. From the growth rate parameters reported in *Table 6*, the ratios of the nucleation constants above and below the break are 1.53 and 2.23 for the blends with 90 and 80 wt% PEO, respectively, whereas values in the vicinity of 2 are expected from theoretical considerations if a transition regime occurs[38,48]. Undoubtedly, careful morphological studies by means of X-ray scattering techniques, concerning the determination of the planes of growth as well as the lamellar thickness behaviour, will offer valuable insight on the true origin of the break in the secondary nucleation plot of the blends.

CONCLUSIONS

A systematic study of the crystallization and melting behaviour of PEO/PVPh blends has been performed over a wide range of compositions and crystallization temperatures. Glass transition results suggest that PVPh is miscible with PEO across the entire range of compositions. The presence of hydrogen-bonding interactions between components leading to miscibility was supported by the large negative value of the interaction energy density determined from both d.s.c. and t.o.a. measurements of the melting point depression. The crystallization process was strongly influenced by the presence of the miscible amorphous component. Thus, the degree of crystallinity and the spherulitic morphology of PEO in the blends, as well as the spherulite growth rate and the overall rate of crystallization, showed a clear composition dependence. Analysis of the isothermal crystallization in terms of the Avrami equation led to values of the Avrami index of 2.5 for both pure PEO and the PEO/PVPh 90/10 blend, whereas a value close to 3 was found for the remaining compositions investigated. The growth data of pure PEO and PEO/PVPh blends have been rationalized in terms of the nucleation and diffusion mechanisms, the latter by means of two mobility factors accounting for the substrate nucleation and the surface spreading processes. A discontinuity in the temperature coefficient of the growth rate curve was found for PEO/PVPh blends with 90 and 80 wt% PEO.

ACKNOWLEDGEMENTS

We are pleased to acknowledge financial support of this work by the Diputación Foral de Gipuzkoa (Programa Marco de Apoyo a la PYME 1992). We would also thank R. Hernández and J. del Val for assistance with the d.m.t.a. and WAXD measurements, respectively.

REFERENCES

1 Olabisi, O., Robeson, L. M. and Shaw, M. T. 'Polymer–Polymer Miscibility', Academic Press, New York, 1979
2 Paul, D. R. and Newman, S. 'Polymer Blends', Academic Press, New York, 1978
3 Coleman, M. M., Graf, J. F. and Painter, P. C. 'Specific Interactions and the Miscibility of Polymer Blends', Technomic Publishing Company, Lancaster, PA, 1991
4 Sperling, L. H. 'Introduction to Physical Polymer Science', John Wiley & Sons, New York, 1986
5 Calahorra, M. E., Cortázar, M. and Guzmán, G. M. *Polym. Commun.* 1983, **24**, 211
6 Pedemonte, E., Turturro, A. and Semino, G. *Thermochim. Acta* 1988, **137**, 115
7 Nishi, T. and Wang, T. T. *Macromolecules* 1975, **8**, 909
8 Rim, P. B. and Runt, J. P. *Macromolecules* 1984, **17**, 1520
9 Martuscelli, E. *Polym. Eng. Sci.* 1984, **24**, 563
10 Alfonso, G. C. and Russell, T. P. *Macromolecules* 1986, **19**, 1143
11 Saito, H., Okada, T. and Inoue, T. *Macromolecules* 1991, **24**, 4446
12 Okada, T., Saito, H. and Inoue, T. *Polymer* 1993, **34**, 4752
13 Smith, K. L., Winslow, A. E. and Peterson, D. E. *Ind. Eng. Chem.* 1959, **51**, 1361
14 Osada, Y. and Sato, M. *J. Polym. Sci., Polym. Lett. Edn* 1976, **14**, 129
15 Robeson, L. M., Hale, W. F. and Merian, C. N. *Macromolecules* 1981, **14**, 1644
16 Iriarte, M., Iribarren, J. I., Etxeberria, A. and Iruin, J. J. *Polymer* 1989, **30**, 1160
17 Quintana, J. R., Cesteros, L. C., Peleteiro, M. C. and Katime, I. *Polymer* 1991, **32**, 2793
18 Cortázar, M., Calahorra, M. E. and Guzmán, G. M. *Eur. Polym. J.* 1982, **18**, 165
19 Marco, C., Fatou, J. G., Gómez, M. A., Tanaka, H. and Tonelli, A. E. *Macromolecules* 1990, **23**, 2183
20 Kalfoglou, N. K. *J. Polym. Sci., Polym. Phys. Edn* 1982, **20**, 1259
21 Walsh, D. J. and Sinmh, V. B. *Makromol. Chem.* 1984, **185**, 1979
22 Cesteros, L. C., Quintana, J. R., Fernández, J. A. and Katime, I. *J. Polym. Sci., Polym. Phys. Edn* 1989, **27**, 2567
23 Moskala, E. J., Varnell, D. F. and Coleman, M. M. *Polymer* 1985, **26**, 228
24 Qin, Ch., Pires, A. T. N. and Belfiore, L. A. *Polym. Commun.* 1990, **31**, 177
25 Zhang, X., Takegoshi, K. and Hikichi, K. *Macromolecules* 1992, **25**, 2336
26 Avrami, M. *J. Chem. Phys.* 1939, **7**, 1103
27 Avrami, M. *J. Chem. Phys.* 1940, **8**, 212
28 Avrami, M. *J. Chem. Phys.* 1941, **9**, 177
29 Van Krevelen, D. W. 'Properties of Polymers', Elsevier, Amsterdam, 1990
30 Ferry, J. D. 'Viscoelastic Properties of Polymers', 3rd Edn, Wiley, New York, 1980
31 Pedrosa, P., Pomposo, J. A., Calahorra, E. and Cortázar, M. *Macromolecules* 1994, **27**, 102
32 Harris, J. E., Goh, S. H., Paul, D. R. and Barlow, J. W. *J. Appl. Polym. Sci.* 1982, **27**, 839

33 Scott, R. L. *J. Chem. Phys.* 1949, **17**, 279
34 Hoffman, J. D. and Weeks, J. J. *Res. Nat. Bur. Stand.* 1962, **66**, 13
35 Mezghani, K., Campbell, R. A. and Phillips, P. J. *Macromolecules* 1994, **27**, 997
36 Martuscelli, E., Pracella, M. and Yue, W. P. *Polymer* 1984, **25**, 1907
37 Ong, C. J. and Price, F. P. *J. Polym. Sci., Polym. Symp.* 1978, **63**, 45
38 Hoffman, J. D., Davis, G. T. and Lauritzen, J. I. Jr in 'Treatise on Solid-State Chemistry' (Ed. N. B. Hannay), Plenum Press, New York, 1976, Vol. 3, Ch. 7
39 Lauritzen, J. I. *J. Appl. Phys.* 1973, **44**, 4353
40 Frank, F. C. *J. Cryst. Growth* 1974, **22**, 223
41 Doi, M. and Edwards, S. F. 'The Theory of Polymer Dynamics', Oxford University Press, Oxford, UK, 1986
42 Pearson, D. S., Fetters, L. J., Graessley, W. W., Strate, G. V. and Von Meerwall, E. *Macromolecules* 1994, **27**, 711
43 Williams, M. L., Landel, R. F. and Ferry, J. D. *J. Am. Chem. Soc.* 1975, **77**, 3701
44 Cheng, S. Z. D., Chen, J. and Janimak, J. J. *Polymer* 1990, **31**, 1018
45 Hay, J. N. and Sabir, M. *Polymer* 1969, **10**, 187
46 Maclaine, J. Q. G. and Booth, C. *Polymer* 1975, **16**, 191
47 Alfonso, G. C. and Russell, T. P. *Macromolecules* 1986, **19**, 1143
48 Hoffman, J. D. *Polymer* 1983, **24**, 3